

Trinity University

Digital Commons @ Trinity

Physics and Astronomy Faculty Research

Physics and Astronomy Department

2001

Ring Current Ion Composition During Solar Minimum and Rising Solar Activity: POLAR/CAMMICE/MICS Results

T I. Pulkkinen

N Yu Ganushkina

D N. Baker

Niescja E. Turner

Trinity University, nturner1@trinity.edu

J F. Fennell

See next page for additional authors

Follow this and additional works at: https://digitalcommons.trinity.edu/physics_faculty



Part of the [Astrophysics and Astronomy Commons](#)

Repository Citation

Pulkkinen, T.I., Ganushkina, N.Y., Baker, D.N., Turner, N.E., Fennell, J.F., Roeder, J., Fritz, T.A., ... & Kettmann, G. (2001). Ring current ion composition during solar minimum and rising solar activity: Polar/CAMMICE/MICS results. *Journal of Geophysical Research: Space Physics*, 106(A9), 19131-19147. doi: 10.1029/2000JA003036.

This Article is brought to you for free and open access by the Physics and Astronomy Department at Digital Commons @ Trinity. It has been accepted for inclusion in Physics and Astronomy Faculty Research by an authorized administrator of Digital Commons @ Trinity. For more information, please contact jcostanz@trinity.edu.

Authors

T I. Pulkkinen, N Yu Ganushkina, D N. Baker, Niescja E. Turner, J F. Fennell, J L. Roeder, T A. Fritz, M Grande, B Kellett, and G Kettmann

Ring current ion composition during solar minimum and rising solar activity: Polar/CAMMICE/MICS results

T. I. Pulkkinen,¹ N. Yu. Ganushkina,¹ D. N. Baker,² N. E. Turner,^{1,2}
J. F. Fennell,³ J. Roeder,³ T. A. Fritz,⁴ M. Grande,⁵ B. Kellett,⁵ and
G. Kettmann⁶

Abstract. This paper shows statistical results of the ring current ion composition and its variability as a function of solar cycle and magnetospheric activity for $3 < L < 8$. Spin-averaged energetic particle (1–200 keV) measurements from Polar are combined with geomagnetic indices as well as solar wind and interplanetary observations from the Wind spacecraft during a period from September 1996 to March 1999. The statistics are performed both for time-averaged values for all periods as well as for peak flux values during geomagnetic storms (defined as $Dst < -50$ nT) that occurred during this period. The average O^+ energy density increases by about a factor of 5 during the rising phase of the solar cycle from the minimum values in 1996, while the average values of H^+ and He show variability but no consistently increasing trend. The O^+ flux is small (below 10%) compared with the hydrogen flux, and the average energy density ranges from a few percent at solar minimum to $\sim 10\%$ at high solar activity time in early 1999. The O^+ flux is typically smaller than the He^+ flux, reaching comparable values only during the latter part of the period when the solar activity increased. Analogously, the energy densities of O^+ and He^+ are about equal during 1996 and 1997, whereas the O^+ energy density is about twice the He^+ energy density during the higher solar activity period in 1998 and early 1999.

1. Introduction

The plasma population in the inner magnetosphere has two sources, namely, the dense, cold ionosphere and the cool solar wind [Williams, 1987]. The relative importance of these sources, which varies as a function of geomagnetic conditions, can be identified from higher-mass ions: Whereas the solar wind contains alpha particles and small amounts of heavier elements, the ionosphere provides mostly singly charged helium and oxygen in addition to hydrogen. The relative importance of these sources is also a function of location: The inner magnetosphere is dominated by the ionospheric source,

whereas the outer magnetosphere is solar wind dominated [e.g., Winglee, 1998].

The outflow of ionospheric ions is largely controlled by the thermospheric temperature, which varies both on short timescales as a response to geomagnetic activity as well as over the solar cycle. Both magnetospheric substorms and geomagnetic storms heat the thermosphere and hence lead to enhancement of the ionospheric ion outflow from the dayside cleft ion fountain [Cladis, 1986] and from the nightside auroral zone [Daglis *et al.*, 1994]. On the other hand, increase in the solar UV irradiance can increase the thermospheric temperature by a factor of 4 at solar maximum relative to the temperature during solar minimum [Moore *et al.*, 1999], which leads to generally more ionospheric plasma-rich magnetosphere during the solar maximum [Young *et al.*, 1982].

The inner magnetosphere consists of several distinct plasma populations: the cold plasmasphere, the energetic particles in the radiation belts, the hot ring current, and the inner edge of the plasma sheet are all partially colocated. The ring current is especially important in terms of magnetospheric dynamics, as it largely controls the inner magnetospheric magnetic field configuration. Therefore it is especially interesting to examine how the inner magnetosphere dynamics depends on the composition of the ring current. As the ring current ions have characteristic energies of several tens of

¹Finnish Meteorological Institute, Helsinki, Finland.

²Laboratory for Atmospheric and Space Physics, University of Colorado, Boulder, Colorado.

³The Aerospace Corporation, Los Angeles, California.

⁴Department of Astronomy, Boston University, Boston, Massachusetts.

⁵Rutherford Appleton Laboratory, Didcot, England, United Kingdom.

⁶Max-Planck-Institut fuer Aeronomie, Katlenburg-Lindau, Germany.

Copyright 2001 by the American Geophysical Union.

Paper number 2000JA003036.

0148-0227/01/2000JA003036\$0900

kilovolts, active processes are required to accelerate the ions from the source temperatures to the observed ring current temperatures [Cladis, 1986; Moore *et al.*, 1999].

Geomagnetic storms are created by a variety of strong disturbances originating from the Sun. For example, coronal mass ejections (CMEs) and the subsequent interplanetary magnetic clouds are characterized by strong and slowly varying interplanetary magnetic field (IMF). When the IMF points southward, CMEs are effective drivers of strong geomagnetic activity [Burlaga, 1991]. One of the main characteristics of geomagnetic storms is the formation of an intense ring current [Hamilton *et al.*, 1988], often with an enhanced ionospheric component present [Kremser *et al.*, 1993; Roeder *et al.*, 1999]. Although strong substorms occur during geomagnetic storms, storms are more than a composite of several substorms [McPherron, 1997].

Both geomagnetic storms and substorms are rich phenomena associated with a number of different processes in various magnetospheric regions. In order to statistically characterize substorms and storms, indices derived from ground magnetic records are often used. Substorms are mostly effective at high latitudes, and hence the substorm intensity is characterized by the auroral electrojet indices AU/AL derived from auroral zone magnetograms or the 3-hour Kp index giving a more time-averaged view of the activity. On the other hand, geomagnetic storms create a strong ring current whose effects can be measured by midlatitude magnetograms. The average disturbance over several stations, the Dst index, is used to characterize the storm intensity. This index is usually given as an hourly average.

The storm and substorm activity vary also on a longer timescale over the 11-year solar cycle. Whereas the substorm activity often shows a two-peaked structure, one slightly before the solar maximum and the other during the early declining phase [Nevalinna and Pulkkinen, 1998], the storm occurrence peaks during the declining phase, when strong geomagnetic activity is driven by coronal mass ejections [Gosling *et al.*, 1991] and high-speed solar wind streams originating from low-latitude coronal holes [Feldman *et al.*, 1978]. The 11-year cycle also causes other variations in the solar effects on Earth, one of the most important for the ionospheric processes being the increase of the UV flux with solar activity, which is a potentially important part of the ionosphere-magnetosphere coupling. The F10.7 radio flux is often used as a proxy for the UV flux variations.

The first three years of operation of the Polar spacecraft allow for detailed examination of the plasma composition during a very quiet period near the solar minimum and during the rising phase of the solar cycle. The Charge and Mass Magnetospheric Ion Composition Measurement / Magnetospheric Ion Composition Sensor (CAMMICE/MICS) [Wilken *et al.*, 1992] is capable of measuring ions roughly in the energy range from 1 to 200 ke, and separating particle species as well as their charge states. The highly elliptical polar orbit with an

18-hour orbital period compromises time resolution but allows for observations at all magnetic L shells above $L = 3$.

In this paper we compare the ion flux measurements to the interplanetary magnetic field and solar wind measurements and to the geomagnetic activity indices. Both average flux values and average energy density values are computed for hydrogen, singly and doubly charged helium, and for singly charged oxygen. The IMF, solar wind, and activity parameters are averaged over the periods when the measurements were made, and the correlation of the flux and energy density values with both the interplanetary drivers and the proxies for geomagnetic activity are examined. A specific goal of the study is to examine the ion composition changes during geomagnetically active periods (especially storms) during different phases of solar activity.

Of the ion species selected for examination, H^+ originates both from the ionosphere and from the solar wind, whereas O^+ comes only from the ionosphere and He^{++} comes only from the solar wind. On the other hand, He^+ can be either of ionospheric or of solar wind origin (He^{++} charge-exchanged). Therefore enhancements of He^+ and He^{++} need to be examined together; here we do not attempt to distinguish the portion of He^+ coming from the charge-exchange processes [Kremser *et al.*, 1993].

2. Data Set

The data used in this study comprise pitch angle averaged fluxes measured by the CAMMICE/MICS instrument [Wilken *et al.*, 1992] on board Polar during September 1, 1996, to March 31, 1999. MICS measures a full distribution function in 96 s, which is why the data were averaged to that resolution. The data are tagged with Polar orbital information and L shell values obtained from the Polar database. Note that the L values do not account for the actual state of the magnetosphere, which can introduce errors in the L value estimations during highly disturbed periods. However, accounting for the actual mapping was not possible, because this has to be done on an event-by-event basis and because there are no good magnetic field models for the storm time inner magnetosphere.

The measured flux, $j(E, L)$, was integrated over all measured energies,

$$J(L) = \int_{E_{\min}}^{E_{\max}} dE j(E, L), \quad (1)$$

to give the total flux, $J(L)$, as a function of L . Furthermore, we compute the average and peak fluxes between $L = 3$ and $L = 8$ for each pass. In the computations the particle pitch angle distributions were assumed to be sufficiently isotropic that within this L range no corrections to equatorial flux values were necessary. Figure 1 shows a sample of the flux values as a function of L

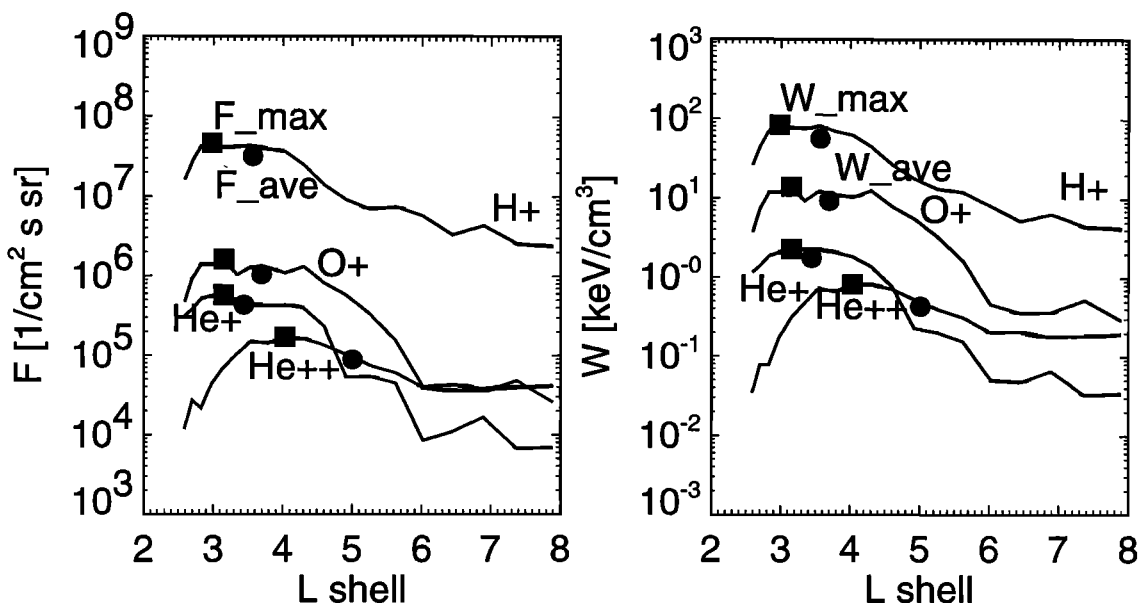


Figure 1. Polar/CAMMICE/MICS observations of H^+ , He^+ , He^{++} , and O^+ ions during a geomagnetic storm on October 23, 1996. (left) The flux values as a function of L shell. (right) The energy densities as function of L shell.

on October 23, 1996. Both the maximum and average fluxes are marked in Figure 1 for hydrogen, helium, and oxygen.

If a pitch angle correction were to be applied, the standard way would be to assume a dependence on the pitch angle $j^{eq}(E, \alpha) = j^{meas}(E, \pi/2) \sin^n \alpha$, where j^{eq} and j^{meas} are the equatorial and measured fluxes, and α is the pitch angle. However, detailed examinations of the distribution functions suggested that for the most part, the distributions within the MICS energy range were quite isotropic and that a common anisotropy factor, n , could not be found for the entire data set. Because finding the correct n is quite a complicated process [Roeder *et al.*, 1999], we assumed $n = 0$ in the statistical examination. The result of this approximation leads to a slight underestimation of the fluxes (especially for heavier ions) during storm periods and/or during lower solar activity, when the anisotropy is likely to be larger. On the other hand, n typically becomes large only for energies much higher than those covered by the CAMMICE/MICS instrument.

Plate 1 shows an overview of the period in question. Plates 1a - 1d show four channels (R0 - R3) of the MICS instrument, H^+ , He^+ , He^{++} , and O^+ , in an L shell - time format, where the total flux intensity is color coded. Plates 1e, 1f, and 1g show flux ratios, O^+/H^+ , O^+/He^+ and O^+/He^{++} . Plates 1h and 1i show the Dst index characterizing the geomagnetic activity conditions, and the $F10.7$ flux indicating the level of solar activity. Storm periods ($Dst < -50$ nT) are marked red in the Dst panel. The $F10.7$ flux clearly shows how the solar activity starts to rise around September 1997 (day 600 in Figure 1b). A similar trend of rising activity is also evident in the Dst data, with more intense

storm activity after September 1997 than during the solar minimum period (September 1996 to September 1997).

The particle fluxes show the bulk of the ring current particles mainly in the region between $L = 4$ and $L = 6$. All species show periodic enhancements, which are coincident with the Dst enhancements and hence associated with geomagnetic storms. Both the solar wind origin He^{++} and ionospheric O^+ are enhanced during storms, although the effects in He^{++} are weaker and the population is generally at higher L values. Note also how the oxygen peaks strongly at relatively low L values ($L < 4$) and how the general level of oxygen increases from the solar minimum toward higher solar activity. Plate 1e shows that the oxygen flux is low relative to the hydrogen flux, typically only a few percent. However, the amount of oxygen increases with the solar activity, but even at the end of the period, the ratio rarely reaches 10%. Similarly, the O^+/He^+ shows that the helium fluxes dominate over the oxygen fluxes, which are typically less than 50% of the helium fluxes. However, as the solar activity increases during 1998 and 1999, the oxygen fluxes can at times rise even over the helium flux values. The O^+ fluxes are always higher than the He^{++} fluxes in the ring current region, as the He^{++} fluxes are largest at higher L shells.

For the statistical examination the mean total flux, J_{ave} , (within the L shell range between $L = 3$ and $L = 8$), the peak total flux, J_{max} , and the L shell where the peak flux was detected, $L_{J,max}$, were tabulated. The L value limits were chosen to restrict the examination only to the ring current region; high energetic ion fluxes can occasionally be found near the dayside magnetopause, but those are not included in this study.

The energy density per unit volume associated with the ring current ions was computed from

$$w(L) = 2\pi\sqrt{2mq} \int_{E_{\min}}^{E_{\max}} dE\sqrt{E}j(E, L), \quad (2)$$

where w is the energy density, m is the ion mass, q is the charge state, and the integral is over energy per unit charge. Also in this case, the mean energy density, w_{ave} , peak energy density, w_{max} , and the L shell where the peak energy density was detected, $L_{w,max}$ were tabulated.

All these observations were tagged with geomagnetic activity parameters, solar wind, and interplanetary magnetic field information. The parameters include the planetary activity index Kp , the Dst index, solar wind velocity, V , and the north-south component of the interplanetary magnetic field, B_Z . Furthermore, to examine the solar wind - magnetosphere coupling, we computed the ϵ parameter [Perreault and Akasofu, 1978] for these periods. All these parameters were averaged over the period during which Polar passed through the ring current region and measured the flux and energy density values. Because of the 18-hour orbit of Polar, it passes through the ring current region relatively quickly, which suggests that for the most part, large temporal changes do not occur during any one pass. On the other hand, owing to the large absences of data at low L values when Polar is near apogee, it is impossible to determine the exact time of formation of the measured particle populations. Therefore any time delays in activity parameters have not been included. Furthermore, 12-hour averages of these parameters were computed such that the 12-hour period ended at the time when Polar completed its ring current crossing. Thus these average values represent the parameters prior to and during the crossings. Finally, the minimum of Dst and the maximum of Kp during each of the 12-hour intervals were determined and used in the correlation analysis.

3. Statistical Results

In order to get an overview of the variations of the ion composition in the inner magnetosphere, the fluxes and energy densities were evaluated for each inner magnetosphere crossing during the time period from September 1, 1996, to March 31, 1999. Plate 1i shows that the data set can be divided into three almost equally long periods characterized by “low solar activity” ($F10.7 < 100$, day of year (DOY) 245–600), “rising solar activity” ($F10.7 \sim 100$, DOY 600–950), and “high solar activity” ($F10.7 > 100$, DOY 950–1186). Differences in these periods thus reflect the changes caused by the longer-term variations in the solar activity.

Figure 2 shows a scatterplot where the hydrogen energy densities have been correlated with the minimum of Dst , average Kp , average V , average B_Z , average ϵ , and the $F10.7$ flux. The Dst minimum and all averages were computed during the 12-hour averaging interval

defined above. The three different periods have been marked with different symbols, squares for DOY 245–600, circles for DOY 600–950, and triangles for DOY 950–1186. Generally, the correlations are not very good, the best ones being the minimum of Dst during the prior 12 hours and the average of Kp during the prior 12-hour period. The different years do not show much variability except that the highest $F10.7$ values occur during the last period, which was how the data set was divided. The solar wind velocity gave somewhat better correlation than the IMF B_Z , but neither correlation is above $R \sim 0.5$. Here also the 12-hour average values give better correlations than the instantaneous values during the measurements, but the differences are not large. Surprisingly, neither the ϵ parameter measuring the efficiency of the solar wind entry nor the $F10.7$ measuring the ionospheric upflow activity show any correlation with the hydrogen energy density. For all these results the correlations are slightly better for the energy density values than for the averaged flux values.

The energy densities for the other species are, of course, smaller than those for the dominant hydrogen, but can be at times quite significant. Figure 3 shows the statistics for the minimum of Dst , the average of Kp , the average of solar wind velocity, and $F10.7$ flux for He^+ , He^{++} , and O^+ . For the Dst index the correlation is best for oxygen, indicating its importance in geomagnetic storms which will be discussed in more detail below. Surprisingly, the best correlation with geomagnetic activity (Kp) is given by the doubly charged (solar wind origin) helium. This is probably due to the inward penetration of the plasma sheet, where the solar wind helium has access to. This might be taken to indicate that He^{++} would correlate well with the ϵ parameter, but this is not the case; the correlations are quite low, similar to those for H^+ (not shown). On the other hand, the solar wind velocity correlation is best for helium. Note also that the range of energy density values for low activity levels is much wider for O^+ than for the other species. This also shows a clear solar activity dependence: The low energy density levels tend to concentrate on the period of low solar activity. The $F10.7$ flux correlations are poor in all cases but are somewhat larger for oxygen (0.33) than for the other species (≤ 0.1), which is one illustration of the increase of the oxygen energy densities as the solar activity increases.

It is interesting to note that all the correlations, if computed for the three time periods separately, show the best correlations for the period of rising solar activity (September 1997 to September 1998). The reason for this is not clear, but it is quite consistent in correlations with all the driver and activity parameters, both for the energy densities and for the averaged flux values.

The long-term energy density content of the ring current is examined in Figure 4 in terms of 27-day running averages of the measured fluxes. Figures 4a - 4d show each of the species separately, whereas the ratios of the

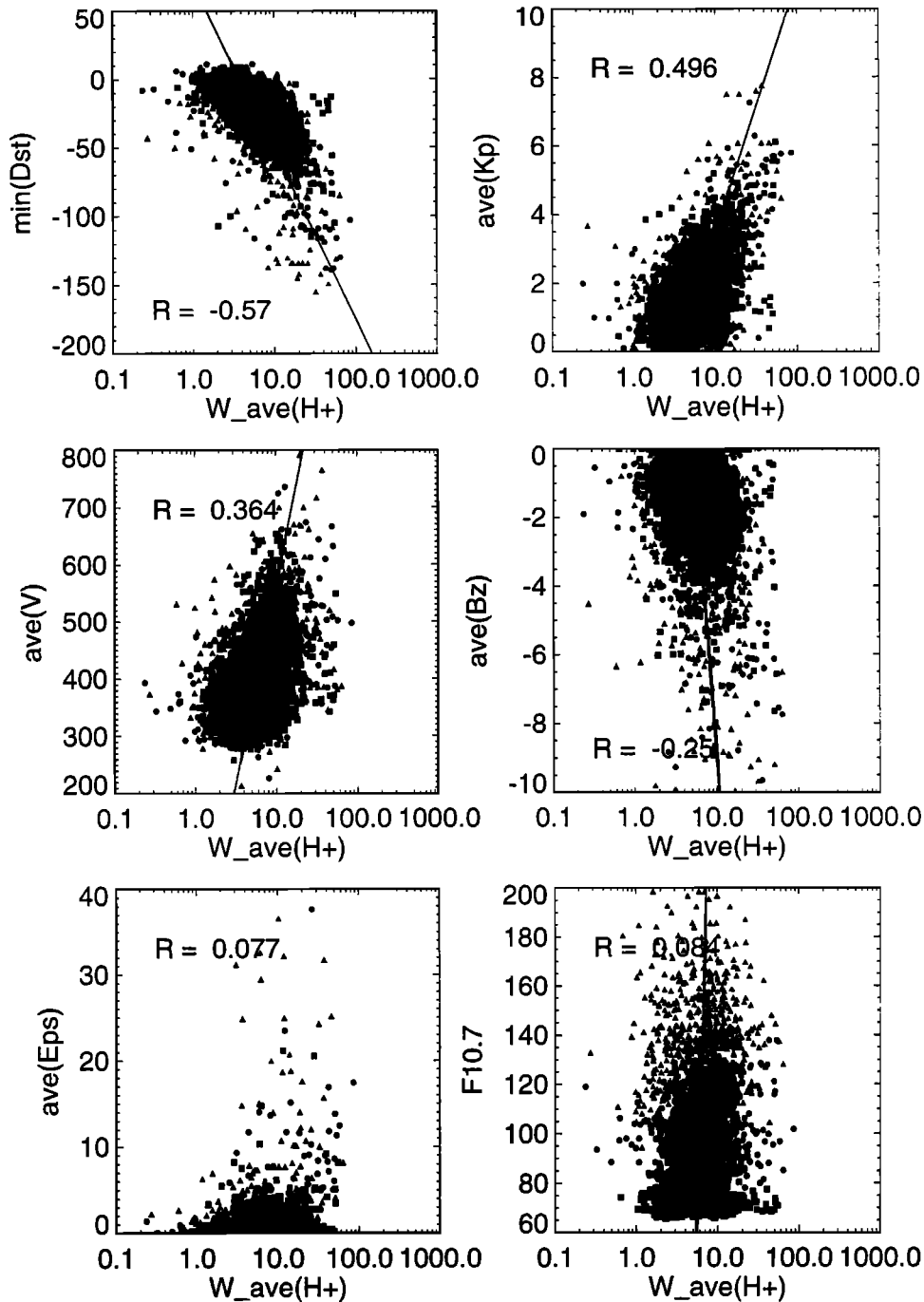


Figure 2. Scatterplots of H^+ energy density (in keV cm^{-3}) versus the minimum of Dst , average of Kp , solar wind velocity, IMF B_Z , ϵ parameter, and the $F10.7$ flux. The different years are shown with different symbols (squares for 1996-1997, circles for 1997-1998, and triangles for 1998-1999).

heavier elements to hydrogen and to singly charged helium are plotted in Figures 4e and 4f. It can be seen that both He^+/H^+ and O^+/H^+ ratios increase as the solar activity increases, but that the increase in the oxygen energy density is much more significant. The relative O^+ energy density is typically around 3% during the solar minimum, whereas it increases to around 10% during higher solar activity. This is evident also

from the flux values in Figure 4d as well as from Figure 4f showing the increasing significance of oxygen as the activity increases. The energy densities of O^+ and He^+ are almost equal during the solar minimum period, but for the higher activity period the O^+ energy density is about twice the He^+ energy density, even though the fluxes are smaller, as was shown in Plate 1. The He^{++} to H^+ ratio did not increase substantially, and

the portion of He^{++} remained small in the inner magnetosphere throughout the period. The vertical bars show the standard errors (standard deviation divided by the square root of the number of samples, shown for every tenth data point to avoid crowding of the plot).

4. Storm Periods

As the largest enhancements of the ionospheric plasma component occur during geomagnetic storms, the entire data set was searched to examine these periods sepa-

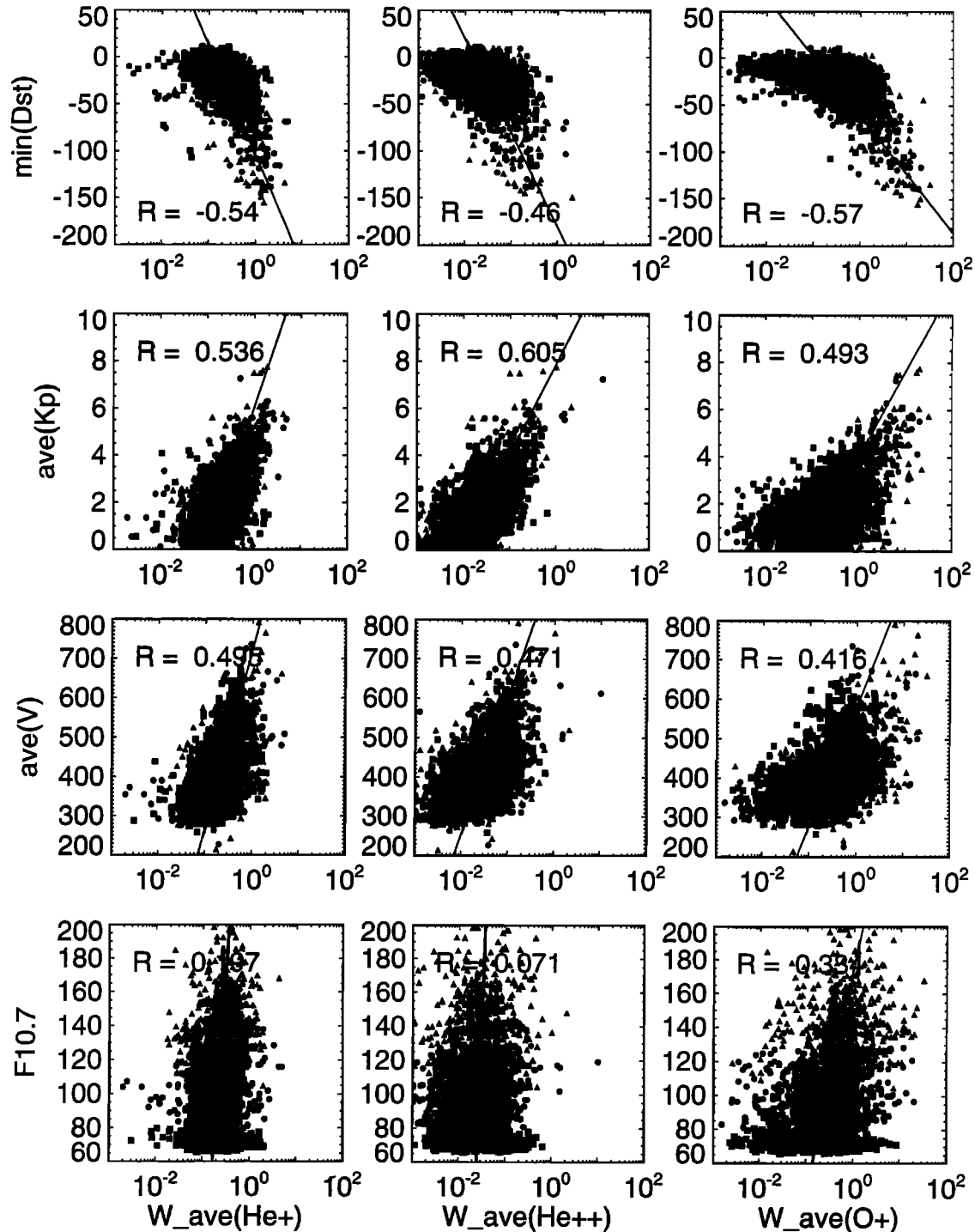


Figure 3. Scatterplot of He^+ , He^{++} , and O^+ energy densities versus the minimum of Dst , average of Kp , average of the solar wind velocity, and $F10.7$. Different years are shown with different symbols (squares for 1996-1997, circles for 1997-1998, and triangles for 1998-1999).

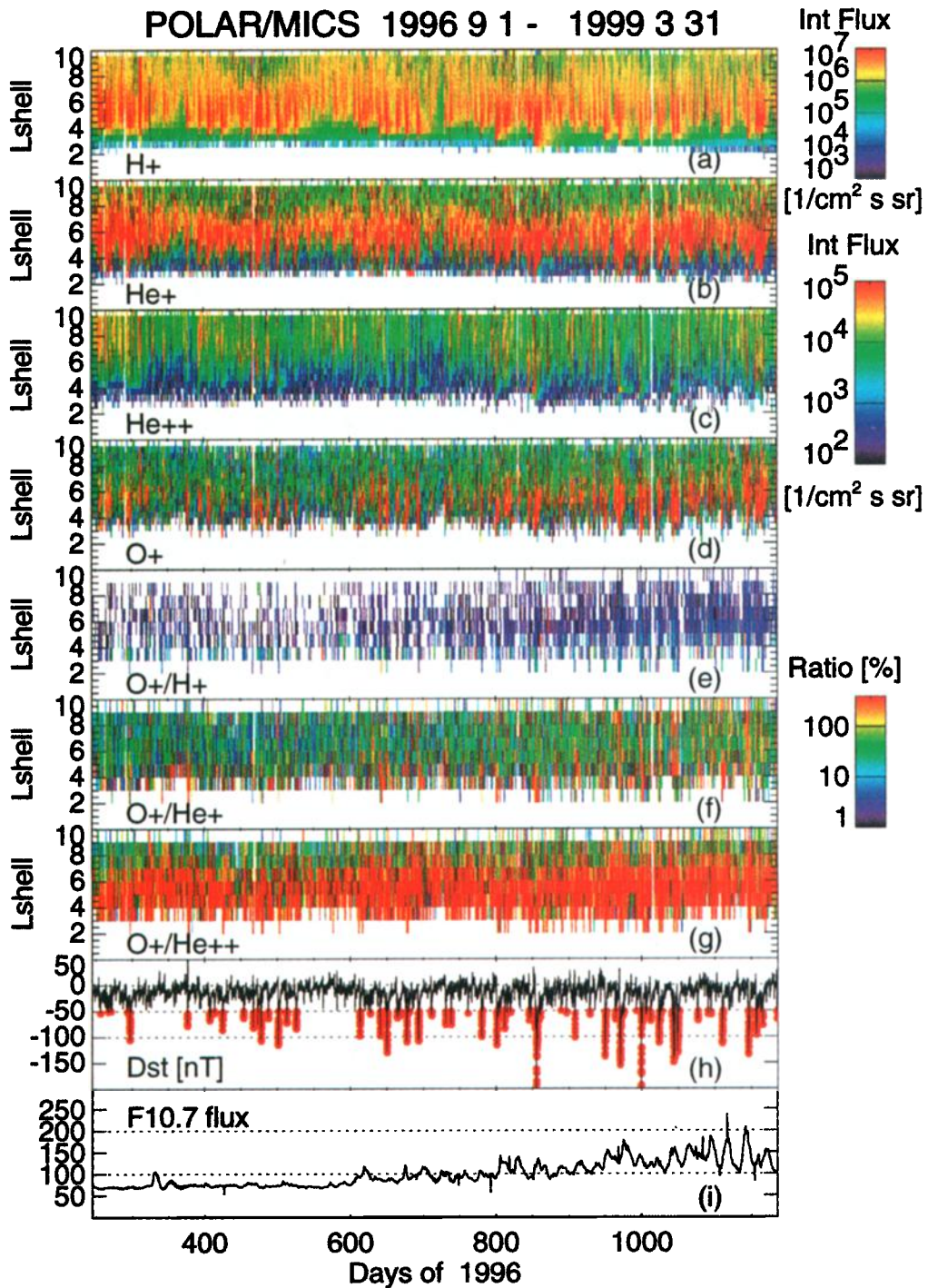


Plate 1. Polar The Charge and Mass Magnetospheric Ion Composition Measurement / Magnetospheric Ion Composition Sensor (CAMMICE/MICS) measurements of the integrated flux versus time and L shell over the period from September 1, 1996 to March 31, 1999. (a) H^+ , (b) He^+ , (c) He^{++} , (d) O^+ , (e) flux ratio O^+/H^+ , (f) flux ratio O^+/He^+ , (g) flux ratio O^+/He^{++} , (h) Dst index, and (i) $F10.7$ flux. Note that the scale for H^+ is different from the other ion species. The time is given in days of year 1996.

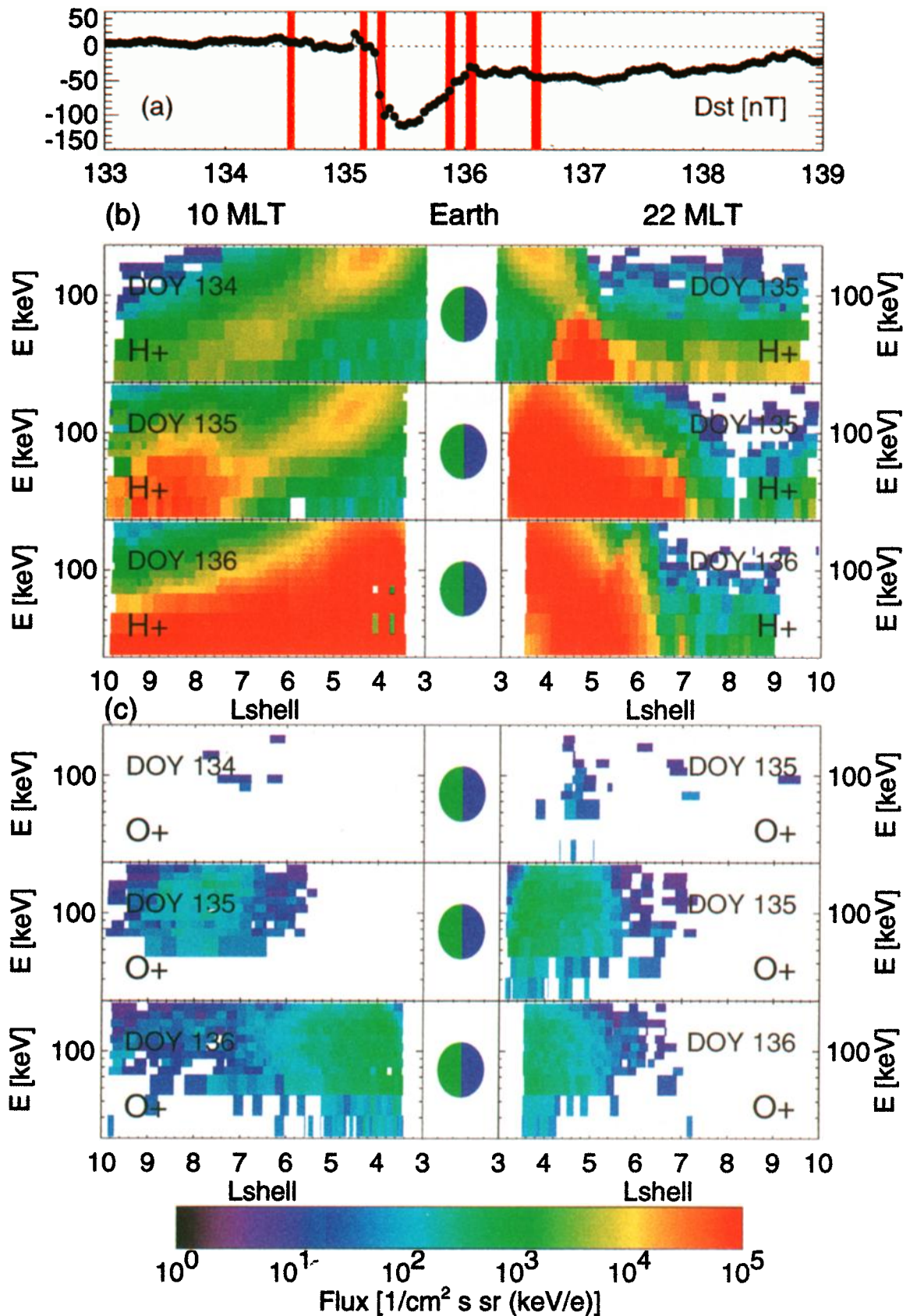


Plate 2. (a) *Dst* index during the storm on May 15, 1997. (b) Polar/MICS energy - *L* shell spectrograms during a storm on May 15, 1997 for hydrogen. (c) Same as Plate 2b but for oxygen. The times of the observation periods are shown with red bars in the *Dst*-plot.

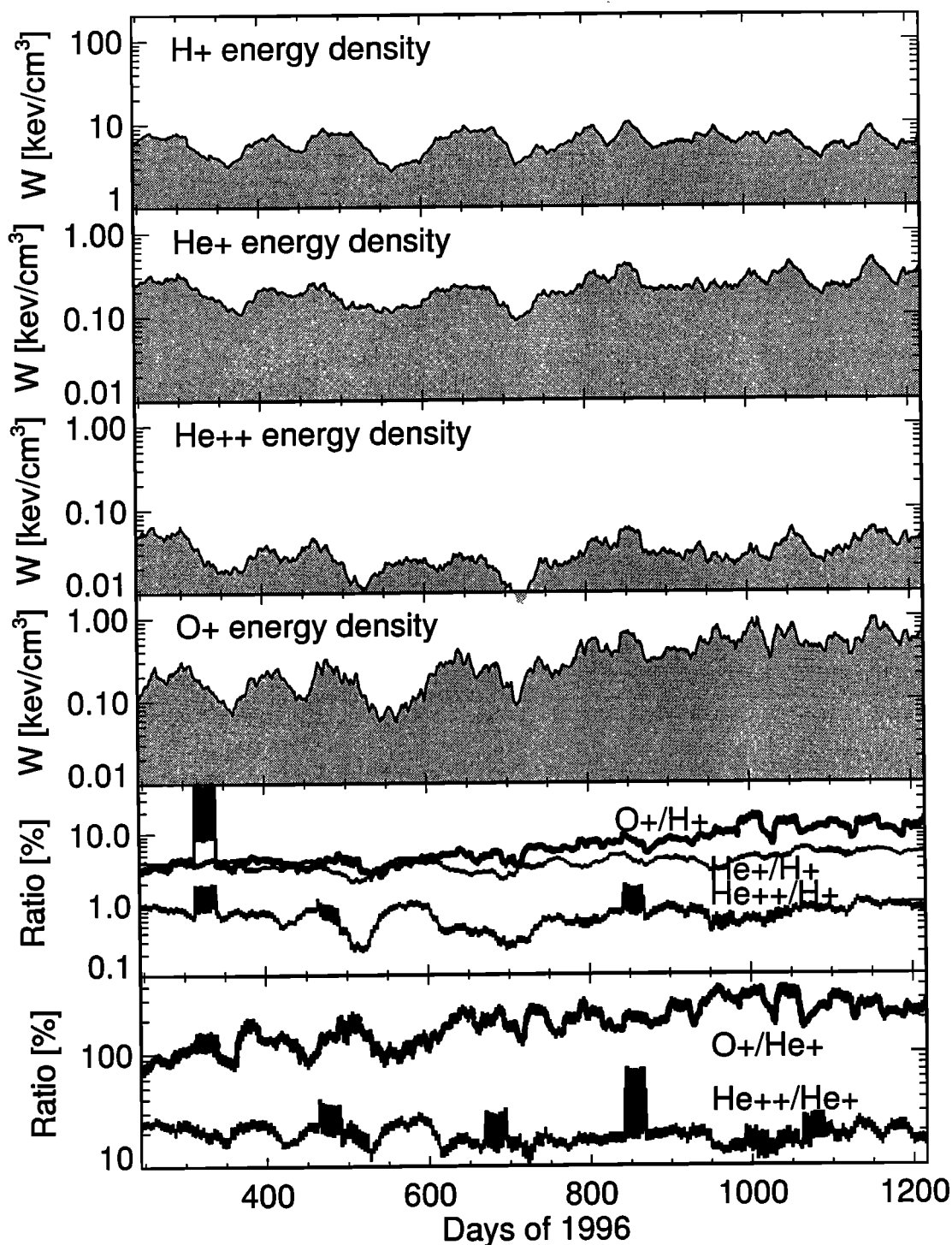


Figure 4. (a-d) Twenty-seven-day averaged values of the energy densities for H^+ , He^+ , He^{++} , and O^+ . (e, f) Ratios of these averaged values of the energy densities for O^+/H^+ , He^+/H^+ , He^{++}/H^+ , O^+/He^+ and He^{++}/He^+ . The vertical bars show the standard errors.

rately. Storms were defined as periods with a minimum of Dst less than -50 nT and were selected by manual inspection of the Dst records available from the World Data Center in Kyoto. In total, 44 storm events were included in the study. Some periods with extended Dst activity around -50 nT were excluded from the study because they did not show a clear peak or typical storm

time behavior. Similarly, peaks during the recovery phases of storms were not counted as separate events.

As an example, Plate 2 shows energy - L spectrograms from several consecutive passes during the May 15, 1997, storm period. Plate 2a shows the Dst index. The red lines mark the periods during which the data shown in panels 2b and 2c were recorded. Plates 2b and

2c show the spectrograms in a format where the dayside (1000 magnetic local time (MLT)) passes are on the left and the nightside (2200 MLT) passes are on the right. Plate 2b shows the hydrogen fluxes, and Plate 2c shows the oxygen fluxes. Notice the first strong enhancement at low energies during the storm main phase, whereas the strongest intensification at ring current energies was reached after the *Dst* minimum during the storm recovery phase.

The O^+ behavior shows some similarities to the H^+ spectra, but also some differences. During DOY 134 there is very little O^+ in the magnetosphere. Shortly after the storm onset (first pass on DOY 135), O^+ appears with the intensification of low-energy H^+ but extending to much higher energies. The lack of O^+ at low energies is probably due to the low sensitivity of the instrument in this energy range. Furthermore, in the next dayside pass, it seems that the O^+ population is located closer to the Earth than the lower-energy H^+ (tens of keV) but farther away than the higher-energy H^+ (around and above 100 keV), which extends all the way to the innermost distance covered by the measurements. The different locations of the H^+ and O^+ populations might

be indicative of separate acceleration processes at different distances or different injection locations in the tail.

In the statistical examination we consider the first Polar crossings through the ring current region after the minimum of *Dst* was reached, that is, measurements that were made as close as possible to the ring current maximum intensity. In the event shown above, this would be the pass well into the storm recovery. This outlines one of the problems in this correlation study: Data from the maximum activity periods are not always available in this data set.

Figure 5 shows the correlations between the H^+ energy density and the minimum of *Dst*, average of *Kp*, average of the solar wind speed, and the *F*10.7 flux. The data set shows only the measurements closest to (but after) the storm maximum as defined from the minimum of *Dst*. The *Dst* plot still shows quite large variability, and the correlation is actually slightly poorer than it is for the full data set. On the other hand, correlation with *Kp* is better than that for the full data set. It is also clearly seen that the data from the high solar activity period (triangles) make the correlation worse;

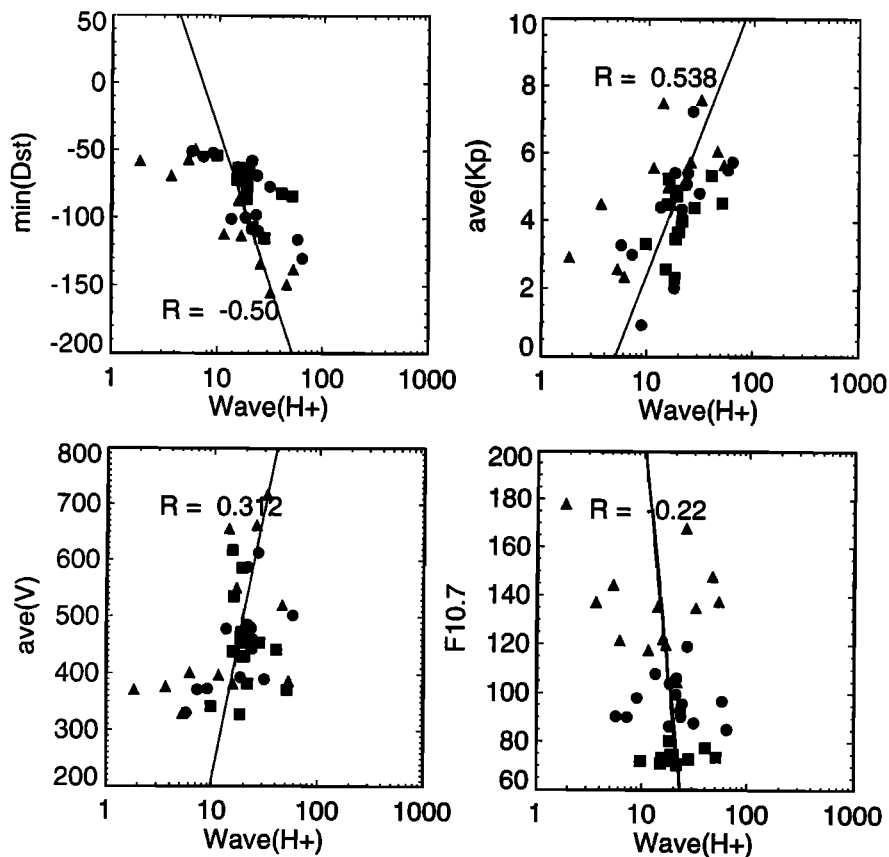


Figure 5. Scatterplots of H^+ energy density versus the minimum of *Dst*, average of *Kp*, solar wind velocity, and the *F*10.7 flux for 44 storms during the examined time interval. The different years are shown with different symbols (squares for 1996-1997, circles for 1997-1998, and triangles for 1998-1999).

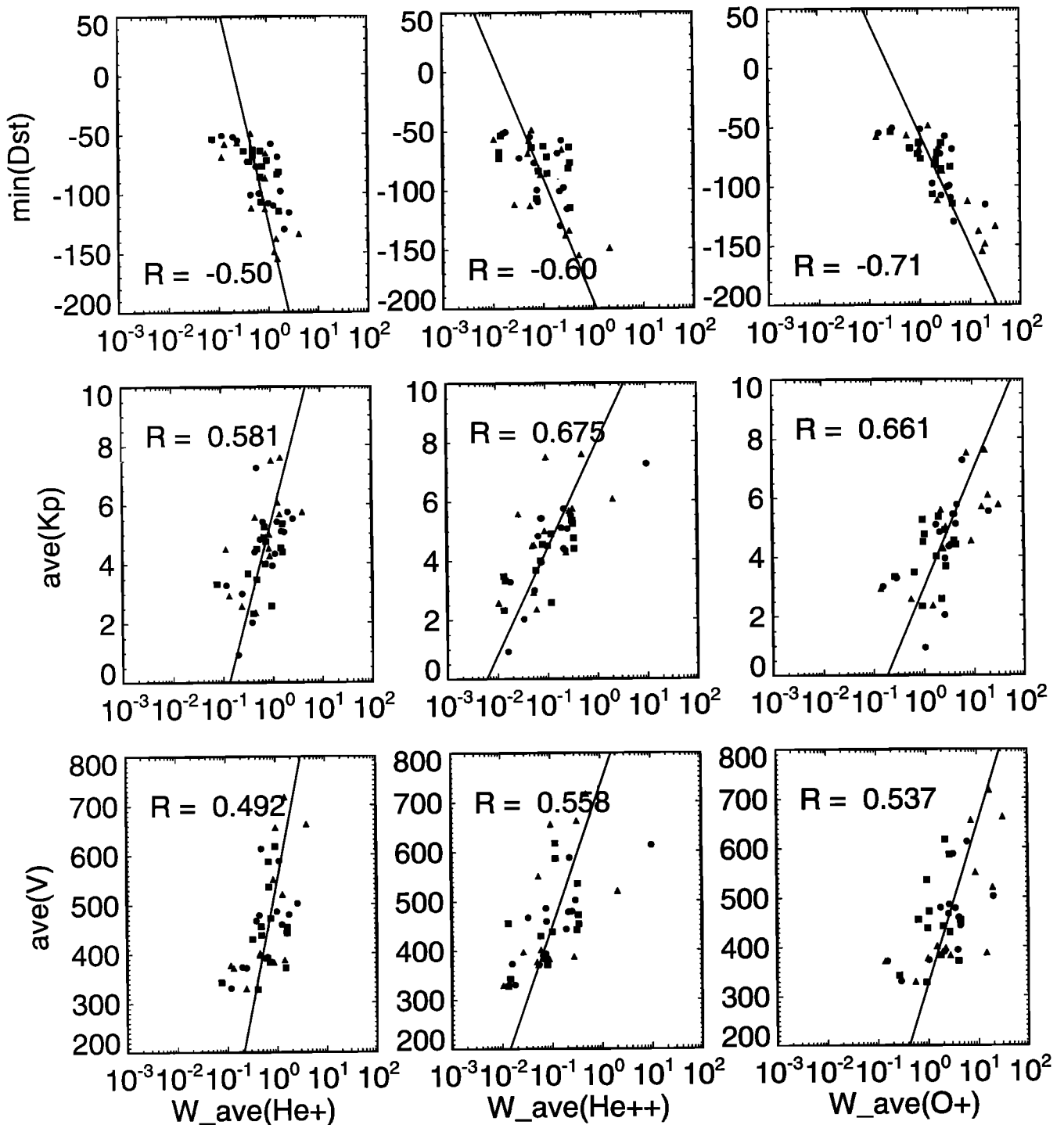


Figure 6. Scatterplot of He^+ , He^{++} , and O^+ energy densities versus the minimum of Dst , average of Kp , and average of the solar wind velocity for 44 storm events during the examined time interval. Different years are shown with different symbols (squares for 1996-1997, circles for 1997-1998 and triangles for 1998-1999).

these periods tend to be characterized by lower fluxes than the other periods.

The picture for the other particle species becomes much more organized when only the storm periods are considered. Figure 6 shows a plot similar to Figure 3, where the helium and oxygen energy densities are correlated with the minimum of Dst , average of Kp ,

and average of solar wind speed. The correlations are clearly higher in almost all cases than those for the full data set. Especially, the O^+ energy density shows good correlation with the Dst minimum.

Even though the activity parameters show a clear correlation with the ring current ion fluxes, the lack of high correlation coefficients points out that the processes in-

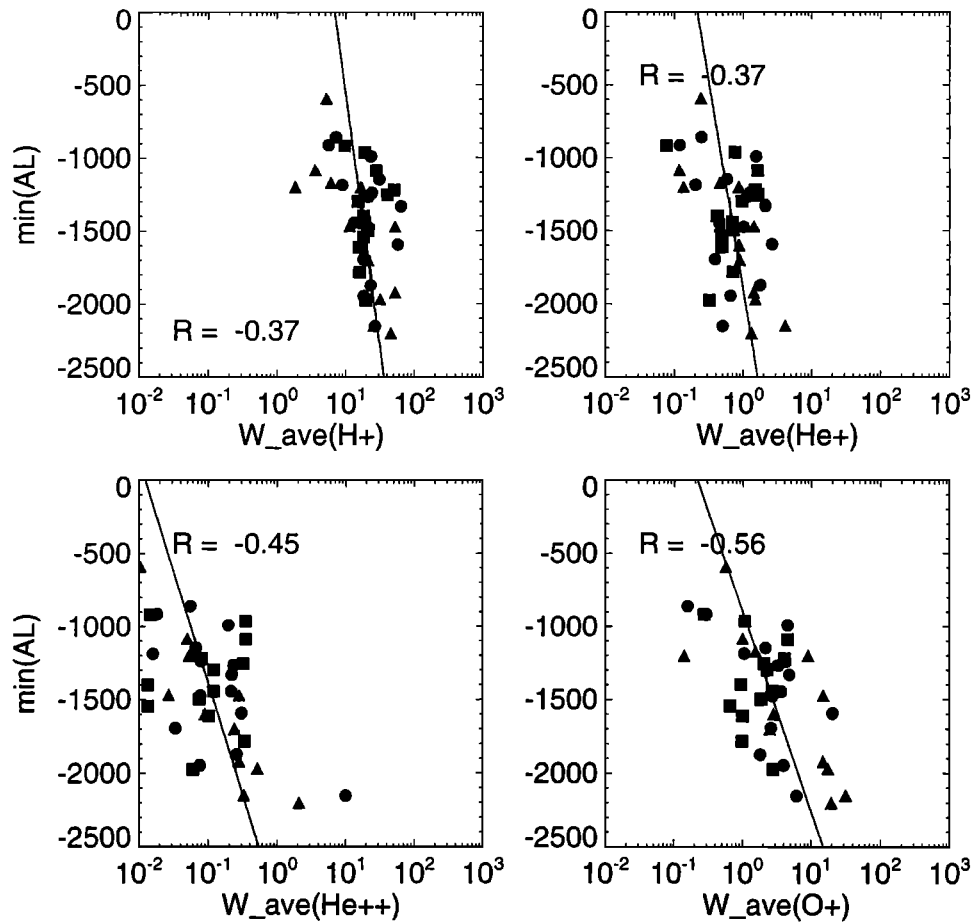


Figure 7. Scatterplot of H^+ , He^+ , He^{++} , and O^+ energy densities versus the minimum of AL index for 44 storm events during the examined time interval. Different years are shown with different symbols (squares for 1996-1997, circles for 1997-1998, and triangles for 1998-1999).

involve multiple aspects and that the resulting ion composition is a function of several factors. Figure 7 shows one more parameter, the minimum of the AL index during the storm period correlated with the average fluxes near the storm maximum. The correlations are not very good for H^+ or He, but the correlation is comparable to the other activity parameters for O^+ .

Figure 8 shows a superposed epoch analysis of the 44 storm events. Figure 8a shows the *Dst* index, and Figures 8b - 8e show the energy densities for H^+ , O^+ , He^+ , and He^{++} . Figures 8f and 8g shows the *L* values where the peak energy densities were recorded. The vertical bars in all panels show the standard errors in the averaging procedure. For the energy density values, the standard errors are, for the most part, small enough that they cannot be distinguished from the plotting symbols. The behavior of the flux values is virtually identical to the energy density values in Figure 8 (not shown).

The *Dst* index reaches its maximum about 12 hours after the initial onset. Note the two-step recovery process, where a more rapid decay after the main phase maximum lasts about 8 hours, and is followed by a slower decay lasting over the entire 8-day period shown

here. It is evident from Figure 8 that all energy density levels rise rapidly after the main phase onset and reach maximum values by the *Dst* minimum time. Whereas the H^+ energy density stays high throughout the 8 days shown in this plot, O^+ , He^+ , and He^{++} decay close to the prestorm values which are shown by the horizontal solid lines. It is also clear that even helium and oxygen decay slowly enough so that they cannot account for the two-step recovery phase. Figure 8f shows the general inward motion of the ring current at storm onset. Whereas the hydrogen energy density maximum stays close to the Earth at slightly outside $L = 4$ after the inward injection, the maximum energy densities of oxygen and helium return to their average higher *L* values within the same time frame as the fluxes decay.

It is interesting to note that the He^{++} values peak already during the main phase whereas the O^+ values increase first after the main phase, but then reach the maximum value only after the initial fast recovery. Similar increase, but a much weaker one, is also evident in the H^+ and He^+ curves. All these increases occur at the time when the *L* values of the peak energy densities reach their lowest values. Thus it is likely that the increase, rather than being a new injection, is associated

with the fact that the particles have had time to transport as far inward as they can under the magnetic and electric fields in the inner magnetosphere. This is also probably associated with the slower decay rate of the *Dst* index at that time.

Comparison of the *Dst* profile with the energy density variations shows that H^+ , He^+ , and O^+ all give a correlation coefficient of about -0.90 , whereas the correlation coefficient for He^{++} is somewhat lower, -0.84 (not shown). Similar comparison of the *L* values of the peak energy densities to the *Dst* profiles gives somewhat lower correlations: for H^+ , only -0.37 , for O^+ , -0.78 , for He^+ , -0.87 , and for He^{++} , -0.81 .

A clear distinction in the correlation coefficients of the ionospheric O^+ and solar wind origin He^{++} would indicate a possible cause for the observed two-step recovery in the *Dst* index: The *L* value changes of the He^{++} energy density maximum would then imply an

inward penetration and a consequent retreat to higher *L* values of the plasma sheet. As the He correlation coefficients are somewhat higher than those for O^+ , this is possibly the case, but further case studies are necessary to confirm this result.

5. Discussion

We have shown in this paper that the ring current ion composition varies significantly from the conditions at solar minimum (1996) to close to the solar maximum (1999): The average O^+ energy density increases by about a factor of 5 during the rising phase of the solar cycle from the minimum values in 1996, and the more frequent storms under these conditions give rise to large peaks in the oxygen and helium concentrations in the inner magnetosphere. On the other hand, the average values of H^+ and He energy densities show variability

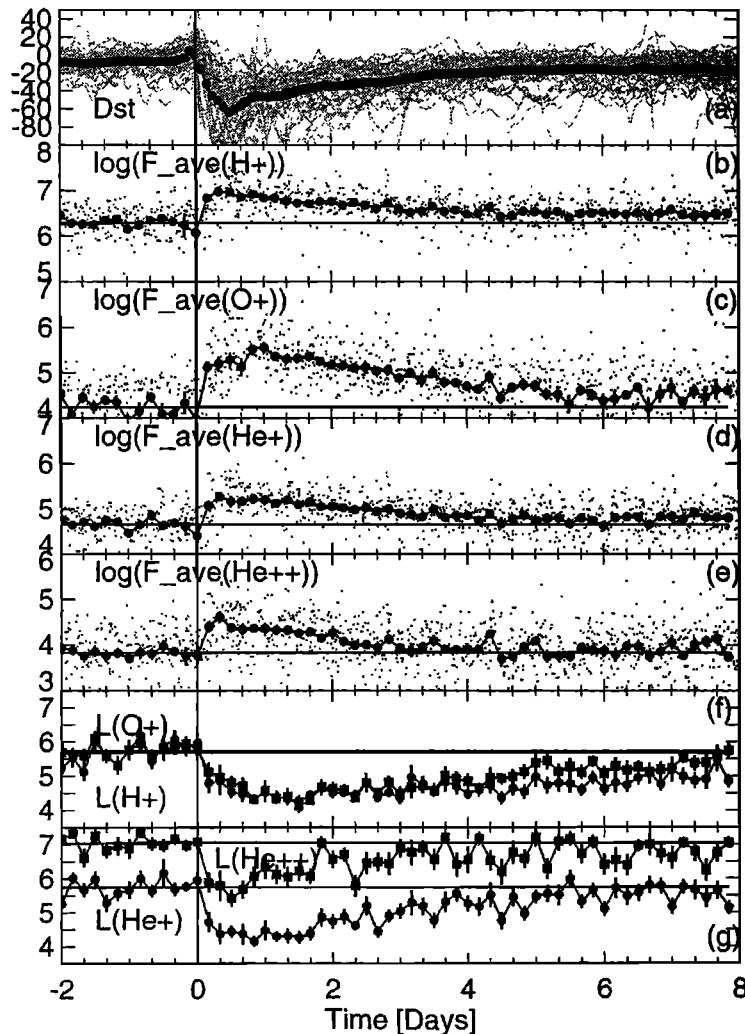


Figure 8. A superposed epoch analysis of the 44 storm events showing (a) the *Dst* index; (b-e) the energy densities of H^+ , He^+ , He^{++} , and O^+ ; (f) the *L*-shell of the peak flux for H^+ and O^+ ; and (g) the *L*-shell of the peak flux for He^+ and He^{++} . The prestorm levels are indicated by the horizontal lines.

but no consistently increasing trend. The O^+ flux is small (below 10%) compared with the hydrogen flux, and the average energy density ranges from a few percent at solar minimum to $\sim 10\%$ at high solar activity time in early 1999. The O^+ flux is typically smaller than the He^+ flux, reaching to comparable values only during the latter part of the period, when the solar activity increased. Analogously, the energy densities of O^+ and He^+ are about equal during 1996 and 1997, whereas the O^+ energy density is about twice the He^+ energy density during the higher solar activity period in 1998 and early 1999. Furthermore, the He^{++} fluxes (and maybe also He^+) show a slight minimum at the end of 1997. Earlier studies have predicted a higher abundance of O^+ in the magnetosphere [e.g., *Daglis et al.*, 1994]. Partly, the differences in the results can be explained by the poor sensitivity of the MICS instrument at low energies: It is possible that a substantial

part of the energy density would be in ions with energies lower than a few tens of keV, which would not be well represented in this study.

The correlation with the geomagnetic activity, solar wind parameters, and overall solar activity is very complex. Generally, the ion fluxes are poorly correlated with the ϵ parameter, even during large storms. This is somewhat surprising, considering the results of *O'Brien and McPherron* [2000], who conclude that the *Dst* activity can be almost completely predicted from the solar wind driver parameters.

The correlation of the ion fluxes with the *F*10.7 fluxes is weaker than one would think, when many previous results have shown that the ionospheric ion outflow is well correlated with the ion fluxes [e.g., *Young et al.*, 1982; *Yau et al.*, 1988; *Moore et al.*, 1999]. Figure 9a shows four frames taken from *Yau et al.* [1988], which give the average response of the ionospheric ion outflow as

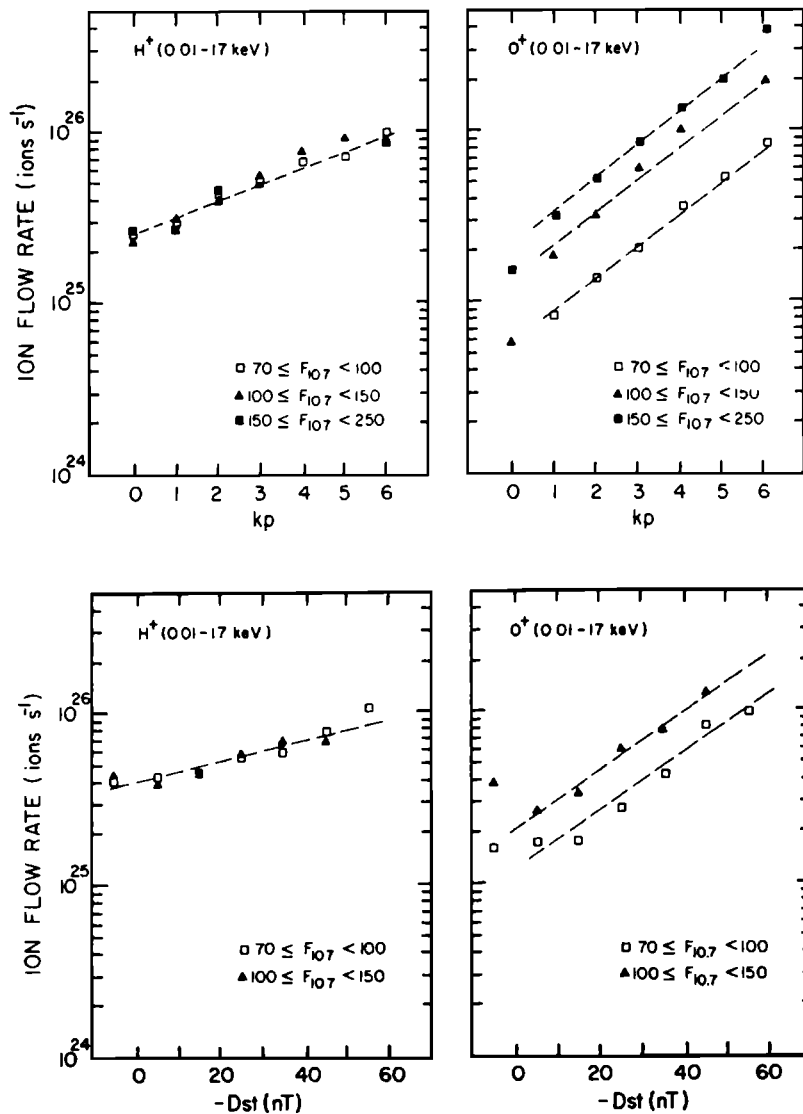


Figure 9a. Ionospheric ion outflow rate of H^+ and O^+ ions at 0.01-17 keV as a function of (top) magnetic *Kp* index and (bottom) *Dst* index for different ranges of *F*10.7 values as measured by Dynamics Explorer 1 during 1981-1986 [from *Yau et al.*, 1988].

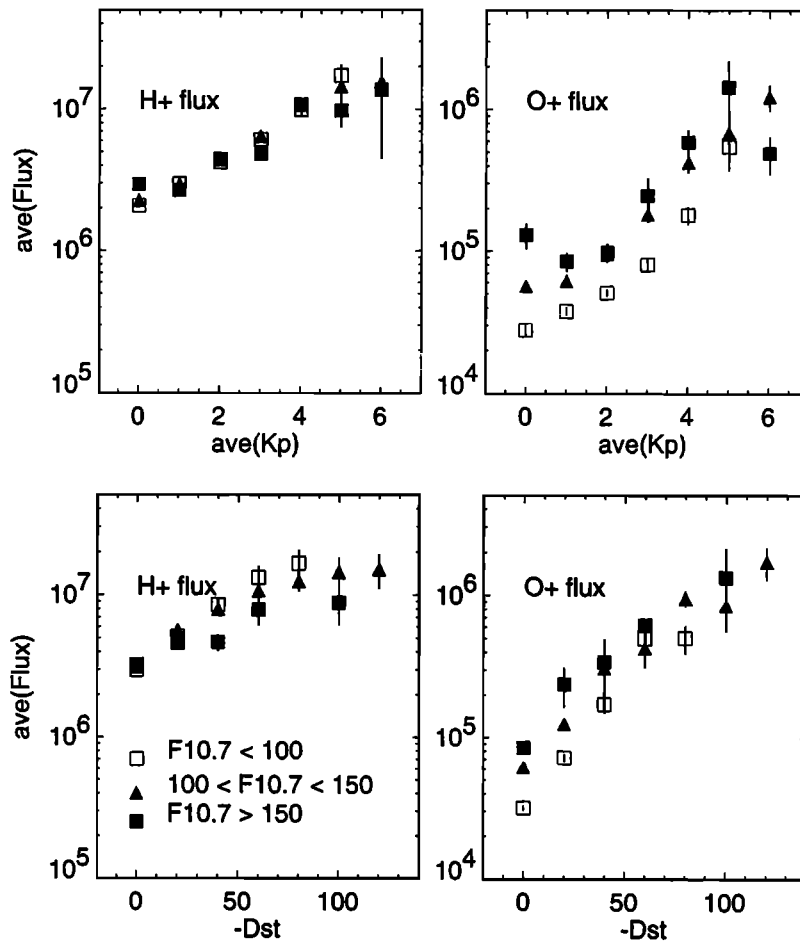


Figure 9b. Ring current H^+ and O^+ ion fluxes at 1-200 keV as a function of (top) magnetic Kp index and (bottom) Dst index for different ranges of $F10.7$ values as measured by Polar/CAMMICE/MICS during 1996-1999. Standard errors are shown with the vertical bars.

measured by the Dynamics Explorer (DE) 1 spacecraft during 1981-1986. Figure 9a shows that the H^+ fluxes increase as a function of activity level (Kp or Dst) but that there is no change for different $F10.7$ flux levels. On the other hand, the O^+ fluxes show clear differences when the data are separated according to the $F10.7$ flux: Separate linear fits can be made which indicate flux levels almost an order of magnitude higher during high $F10.7$ flux than during low solar activity.

Figure 9b shows our measurements of the average energetic H^+ and O^+ fluxes in the magnetosphere at similar intervals of $F10.7$. A similar trend is evident: H^+ fluxes show little correlation with $F10.7$ fluxes, but the O^+ signature is much less clear. First, the trends for increasing activity are not as linear as they are for *Yau et al.* [1988] result, and the differences between the high solar activity and low solar activity are not as clear. Especially, for high activity levels the values are not well separated from each other. This indicates that there are other, more complicated processes which control the acceleration of the ions to the ring current energies. This would suggest that even for a perfect data set, the correlation analysis might not lead to better results. It

appears that some significant effects are introduced in going from the polar outflow region through the equatorial plasma sheet and into the ring current proper.

Observations of lower-energy ions at geosynchronous orbit [*Young et al.*, 1982; *Stokholm et al.*, 1989] show much better correlations between ion densities and the $F10.7$ fluxes than those obtained in this study. The observations made by the European Space Agency's Geosynchronous spacecraft (GEOS 1 and GEOS 2) Ion Composition Experiment used in those studies covered an energy range of 1 - 15 keV, i.e., energies typical for particles that have been accelerated from the auroral region ionosphere to the magnetotail near geosynchronous orbit. On the other hand, the Polar/MICS measurements used in this paper extend to much higher energies and to lower L shells. These measurements are in an energy regime where additional acceleration processes have occurred after the initial acceleration from the ionosphere and in a spatial region where they have been transported from the more distant magnetotail.

The ring current ions enter the inner magnetosphere mainly by radial diffusion from the tail. *Kremser et al.* [1993] used data from the Charge-Energy-Mass

(CHEM) instrument on board the Active Magnetospheric Particle Tracer Explorer / Charge Composition Explorer (AMPTE/CCE) satellite together with a model for radial diffusion. They obtained a good equilibrium between radial diffusion and charge exchange losses for helium inside of $\sim 7 R_E$. On the other hand, *Sheldon and Hamilton [1993]* examined only the very quiet time ring current and concluded that a pure radial diffusion model is not able to account for the observed high fluxes at $L < 4$. They assumed that this discrepancy was due to lack of particle scattering caused by electric field fluctuations in their model. The complex processes that occur during the inward transport of the ions are a likely cause of the large scatter in the correlations obtained in this study.

According to the Dessler - Parker - Sckopke relation [*Dessler and Parker, 1959; Sckopke, 1966*], the energy of the ring current particles is proportional to the ground disturbance of the geomagnetic field with a proportionality

$$\frac{\Delta B}{B_0} = \frac{2W}{3W_m}, \quad (3)$$

where ΔB is the field decrease due to the ring current, B_0 is the average equatorial surface geomagnetic field, $W = \int wdV$ is the total energy of the ring current particles or the energy density integrated over the ring current volume, V , and $W_m \simeq 10^{18}$ J is the energy in the Earth's dipole field above the surface. Assuming that the ring current volume is approximately constant, the ground magnetic disturbance should be proportional to the energy densities measured by Polar/MICS. Figure 10 shows the correlation between the Dst index and the summed energy densities. The correlation coefficient is about the same as it is for the individual species. Thus, different partitioning of the energy density between the different ion species is not responsible for the scatter in the correlations shown in this paper.

To examine the scatter produced by the fact that not all measurements were made near the peak activity, the storm data set was limited to those where the measurement was made within 2 hours of the minimum of Dst . This limited the data set further to only 12 events, but the correlation analyses yielded practically identical results. Assumption of the constant volume is another source for error; however, inclusion of a variable volume would have to be made on an event-by-event basis and is left as a future study.

Part of the scatter in the correlations of course comes from the definition of Dst itself: Instead of being a pure measure of the ring current, it responds to all other magnetospheric current systems as well; the magnetopause current is often corrected by the solar wind dynamic pressure effects [*Burton et al., 1975*], the tail current has been shown to contribute ~ 25 nT close to the time of the substorm onset when the cross-tail current is strong [*Turner et al., 2000*]. Furthermore, the ring current is strongly asymmetric, which then leads to different flux values depending on the longitude at

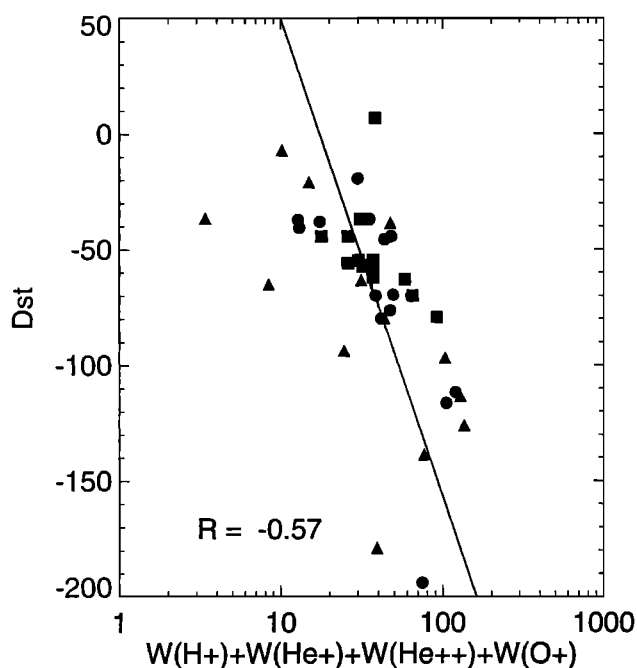


Figure 10. Total ion energy density correlation with Dst index. Different years are shown with different symbols (squares for 1996-1997, circles for 1997-1998, and triangles for 1998-1999).

which the measurements were made. Lastly, the effects caused by induced currents in the ground add about 30% to the measured variation. Given all these factors which affect the Dst measurements in a way different for each event, one would not expect to have a perfect correlation between the Dst and the ring current ion fluxes [see also *Greenspan and Hamilton, 2000*].

It is interesting to note that the O^+ fluxes give the best correlations with the peak of Dst rather than the specific value of the Dst at the time of the flux measurements. This would indicate that strong enhancement of O^+ requires strong substorm activity during the main phase, which could increase the outflow from the ionosphere. However, the peak substorm activity (minimum of AL index) did not show very high correlation coefficient with the oxygen flux. A more thorough evaluation of the substorm activity to the outflow is left as a future study.

Examination of the location of the peak of the energy density showed that the peak moves inward throughout the storm main phase and rapid recovery then stays at the closest location for ~ 1 day, after which the energy density maximum starts to move outward again. The superposed epoch analysis suggests that the most inward location is reached at the time when the Dst decay rate shows a change from the rapid decay to a much slower rate. At this time, especially the oxygen energy density shows a secondary peak. This would indicate that the rapid decay period occurs during the time when the injected population is still being transported inward, whereas the slower recovery would be associated with the time when the peak of the pop-

ulation has already reached the inner magnetosphere around $L = 4$.

In this paper we demonstrate clear changes in the ring current composition and intensity as the solar conditions changed from the minimum toward maximum activity during the 3 years of Polar operations. Polar was launched in a very fortuitous time to record the low fluxes and quiet magnetosphere near the solar minimum, and Polar has continued to produce data until the solar maximum. From the trends here, one can conclude that there are distinct effects that are associated with the long-term solar variability, which is indicative of a solar cycle dependence of the inner magnetosphere trapped population.

The correlation analyses shown here demonstrate that the processes governing the ring current intensity are complex functions of the solar wind driver as well as of the intramagnetospheric processes such as substorms. Therefore the next step in understanding the processes will have to involve detailed analyses of each of the storm events separately, addressing the temporal sequence for each case separately. This is left as a future study.

Acknowledgments. The Wind data used in this study were obtained through the CDAWeb. We thank the PIs of the MFE (J. Slavin) and SWE (A. Lazarus) instruments and the NSSDC for maintaining the CDAWeb facility. The magnetospheric activity indices were obtained from the World Data Center in Kyoto. We thank the referees for valuable suggestions that helped to improve the manuscript.

Janet G. Luhmann thanks John B. Cladis and another referee for their assistance in evaluating this paper.

References

- Burlaga, L. F., Magnetic clouds, in *Physics of the Inner Heliosphere*, p. 1, Springer-Verlag, New York, 1991.
- Burton, R. K., R. L. McPherron, and C. T. Russell, An empirical relationship between interplanetary conditions and *Dst*, *J. Geophys. Res.*, **80**, 4204, 1975.
- Cladis, J. B., Parallel acceleration and transport of ions from polar ionosphere to plasma sheet, *Geophys. Res. Lett.*, **13**, 893, 1986.
- Daglis, I. A., S. Livi, E. T. Sarris, and B. Wilken, Energy density of ionospheric and solar wind origin ions in the near-Earth magnetotail during substorms, *J. Geophys. Res.*, **99**, 5691, 1994.
- Dessler, A. J., and E. N. Parker, Hydromagnetic theory of geomagnetic storms, *J. Geophys. Res.*, **64**, 2239, 1959.
- Feldman, W. C., J. R. Asbridge, S. J. Bame, and J. T. Gosling, Long-term variations of selected solar wind properties: IMP 6, 7 and 8 results, *J. Geophys. Res.*, **83**, 2177, 1978.
- Gosling, J. T., D. J. McComas, J. L. Phillips, and S. J. Bame, Geomagnetic activity associated with Earth passage of interplanetary shock disturbances and coronal mass ejections, *J. Geophys. Res.*, **96**, 7831, 1991.
- Greenspan, M. E., and D. C. Hamilton, A test of the Dessler-Parker-Sckopke relation during magnetic storms, *J. Geophys. Res.*, **105**, 5419, 2000.
- Hamilton, D. C., G. Gloeckler, and F. M. Ipavich, Ring current development during the great geomagnetic storm of February 1986, *J. Geophys. Res.*, **93**, 14 343, 1988.
- Kremser, G., B. Wilken, G. Gloeckler, D. C. Hamilton, F. M. Ipavich, L. M. Kistler, and P. Tanskanen, Origin, transport, and losses of energetic He^+ and He^{++} ions in the magnetosphere of the Earth: AMPTE/CCE observations, *Ann. Geophys.*, **11**, 354, 1993.
- McPherron, R. L., The role of substorms in generation of magnetic storms, in *Magnetic Storms, Geophys. Monogr. Ser.*, Vol. 98, edited by B. T. Tsurutani et al., p. 131, AGU, Washington, D.C., 1997.
- Moore, T. E., R. Lundin, D. Alcaide, M. Andre, S. B. Ganguli, M. Temerin, and A. Yau, Source processes in the high-latitude ionosphere, *Space Sci. Rev.*, **88**, 7, 1999.
- Nevanlinna, H., and T. I. Pulkkinen, Solar cycle correlations of substorm and auroral occurrence frequencies, *Geophys. Res. Lett.*, **25**, 3087, 1998.
- O'Brien, P., and R. L. McPherron, An empirical phase space analysis of ring current dynamics: Solar wind control of injection and decay, *J. Geophys. Res.*, **105**, 7707, 2000.
- Perreault, P., and S.-I. Akasofu, A study of geomagnetic storms, *Geophys. J. R. Astron. Soc.*, **54**, 547, 1978.
- Roeder, J. L., J. F. Fennell, M. Grande, S. Livi, and R. Sheldon, Ring current response to interplanetary magnetic cloud events, *Phys. Chem. Earth*, **24**, 83, 1999.
- Sckopke, N., A general relation between the energy of trapped particles and the disturbance field over the Earth, *J. Geophys. Res.*, **71**, 3125, 1966.
- Sheldon, R. B., and D. C. Hamilton, Ion transport and loss in the Earth's quiet ring current 1, Data and standard model, *J. Geophys. Res.*, **98**, 13 491, 1993.
- Stokholm, M., H. Balsiger, J. Geiss, H. Rosenbauer, and D. T. Young, Variations of the magnetospheric ion number densities near geostationary orbit with solar activity, *Ann. Geophys.*, **7**, 69, 1989.
- Turner, N. E., D. N. Baker, T. I. Pulkkinen, and R. L. McPherron, Evaluation of the tail current contribution to *Dst*, *J. Geophys. Res.*, **105**, 5431, 2000.
- Wilken, B., et al., Magnetospheric ion composition spectrometer onboard the CRRES spacecraft, *J. Spacecr. Rockets*, **29**, 585, 1992.
- Williams, D. J., Ring current and radiation belts, *Rev. Geophys.*, **25**, 570, 1987.
- Winglee, R. M., Multifluid simulations of the magnetosphere: The identification of the geopause and its variation with IMF, *Geophys. Res. Lett.*, **25**, 4441, 1998.
- Yau, A. W., W. K. Peterson, and E. G. Shelley, Quantitative parametrization of energetic ionospheric ion outflow, in *Modeling Magnetospheric Plasma, Geophys. Monogr. Ser.*, Vol. 44, edited by T. E. Moore and J. H. Waite Jr., p. 211, AGU, Washington, D.C., 1988.
- Young, D. T., H. Balsiger, and J. Geiss, Correlations of magnetospheric ion composition with geomagnetic and solar activity, *J. Geophys. Res.*, **87**, 9077, 1982.
- D. N. Baker and N. E. Turner, Laboratory for Atmospheric and Space Physics, University of Colorado, 1234 Innovation Drive, Boulder, CO 80303.
- J. F. Fennell and J. Roeder, The Aerospace Corporation, POBox 92957, Los Angeles, CA 90009.
- T. A. Fritz, Department of Astronomy, Boston University, 725 Commonwealth Ave., Boston, MA 02215.
- N. G. Ganushkina and T. I. Pulkkinen, Finnish Meteorological Institute, POBox 503, FIN-00101 Helsinki, Finland. (tuija.pulkkinen@fmi.fi).
- M. Grande and B. Kellett, Rutherford Appleton Laboratory, Chilton, Didcot, Oxfordshire, OX11, OQX, England, UK.
- G. Kettmann, Max-Planck-Institut fuer Aeronomie, Max-Planck-Str. 2, D-37191 Katlenburg-Lindau, Germany.

(Received May 19, 2000; revised November 6, 2000; accepted November 6, 2000.)